

# Comparative Study of the Optical Properties of $\alpha$ -, $\beta$ -, and $\kappa$ -Ga<sub>2</sub>O<sub>3</sub>

Lewis T. Penman,\* Zak M. Johnston, Paul R. Edwards, Yuichi Oshima, Clifford McAleese, Piero Mazzolini, Matteo Bosi, Luca Seravalli, Roberto Fornari, Robert W. Martin, and Fabien C.-P. Massabuau

A systematic investigation of the optical properties of  $\beta$ -,  $\alpha$ -, and  $\kappa$ -phase gallium oxide (Ga<sub>2</sub>O<sub>3</sub>) polymorphs is conducted by UV–vis spectrophotometry through the Swanepoel method and temperature-dependent photoluminescence. Using the same approach and apparatus allows similarities and differences between these three phases to be directly established. Differences between polymorphs are observed, including refractive indices of 1.89 ( $\beta$ ), 2.00 ( $\alpha$ ), and 1.85 ( $\kappa$ ) and optical bandgaps of 4.99 eV ( $\beta$ ), 5.32 eV ( $\alpha$ ), and 4.87 eV ( $\kappa$ ). In the luminescence studies, four emission peaks in each polymorph are revealed, located at different energies in the UV (3.1–3.9 eV), blue (2.7–3.0 eV), and green (2.2–2.6 eV) regions, with causes attributed to self-trapped holes, donor–acceptor pair transitions involving Ga and O vacancies ( $V_{\text{Ga}}$ ,  $V_{\text{O}}$ ), Ga–O divacancies ( $V_{\text{Ga}} + V_{\text{O}}$ ), O interstitials ( $O_{\text{i}}$ ), and H impurities ( $V_{\text{Ga}}-n\text{H}$ ,  $H_{\text{i}}$ ,  $H_{\text{o}}$ ). In this systematic study, unique optical properties of the different Ga<sub>2</sub>O<sub>3</sub> polymorphs are highlighted and it is warned that the commonly practiced analogy to  $\beta$ -Ga<sub>2</sub>O<sub>3</sub> can lead to misinterpretations.

## 1. Introduction

Gallium oxide (Ga<sub>2</sub>O<sub>3</sub>) is one of the leading wide bandgap semiconductor candidates for applications in high-power electronics and UV optoelectronics.<sup>[1]</sup> Ga<sub>2</sub>O<sub>3</sub> is a highly polymorphic compound, with the main phases labeled  $\beta$ -Ga<sub>2</sub>O<sub>3</sub> (monoclinic),  $\alpha$ -Ga<sub>2</sub>O<sub>3</sub> (rhombohedral), and  $\kappa$ -Ga<sub>2</sub>O<sub>3</sub> (orthorhombic) which is also known as orthorhombic  $\varepsilon$ -Ga<sub>2</sub>O<sub>3</sub><sup>[2,3]</sup> as illustrated in Figure 1. The  $\beta$ -phase has attracted most of the research effort as it is the thermodynamically stable phase.<sup>[4]</sup> Meanwhile, the metastable  $\alpha$ - and  $\kappa$ -phases have recently sparked renewed interest due to the wider bandgap of 5.3 eV for the  $\alpha$ -phase<sup>[5]</sup> and the intrinsic polarization of the  $\kappa$ -phase,<sup>[6,7]</sup> which open new perspectives for high power devices such as high electron mobility transistors (HEMT).<sup>[8,9]</sup> Additionally,  $\alpha$ -Ga<sub>2</sub>O<sub>3</sub> can be used for wide-bandgap engineering with other rhombohedral sesquioxides (e.g., Al<sub>2</sub>O<sub>3</sub>, In<sub>2</sub>O<sub>3</sub>, Fe<sub>2</sub>O<sub>3</sub>, Ti<sub>2</sub>O<sub>3</sub>), which is desirable due to the low lattice mismatch and wide range of achievable bandgaps.<sup>[10]</sup> However, little is known about the optical properties of the  $\alpha$ - and  $\kappa$ -phases, which are often assumed by analogy to be similar to those of  $\beta$ -Ga<sub>2</sub>O<sub>3</sub>. A consistent comparative study of the optical properties of  $\alpha$ -,  $\beta$ -, and  $\kappa$ -Ga<sub>2</sub>O<sub>3</sub> is needed, as each phase's unique structure implies distinct properties. Accurate knowledge of these properties would be an essential aid in the design and fabrication of Ga<sub>2</sub>O<sub>3</sub>-based optoelectronic devices for applications such as solar-blind photodetectors.<sup>[11,12]</sup>

mobility transistors (HEMT).<sup>[8,9]</sup> Additionally,  $\alpha$ -Ga<sub>2</sub>O<sub>3</sub> can be used for wide-bandgap engineering with other rhombohedral sesquioxides (e.g., Al<sub>2</sub>O<sub>3</sub>, In<sub>2</sub>O<sub>3</sub>, Fe<sub>2</sub>O<sub>3</sub>, Ti<sub>2</sub>O<sub>3</sub>), which is desirable due to the low lattice mismatch and wide range of achievable bandgaps.<sup>[10]</sup> However, little is known about the optical properties of the  $\alpha$ - and  $\kappa$ -phases, which are often assumed by analogy to be similar to those of  $\beta$ -Ga<sub>2</sub>O<sub>3</sub>. A consistent comparative study of the optical properties of  $\alpha$ -,  $\beta$ -, and  $\kappa$ -Ga<sub>2</sub>O<sub>3</sub> is needed, as each phase's unique structure implies distinct properties. Accurate knowledge of these properties would be an essential aid in the design and fabrication of Ga<sub>2</sub>O<sub>3</sub>-based optoelectronic devices for applications such as solar-blind photodetectors.<sup>[11,12]</sup>

## 2. Background

### 2.1. $\beta$ -Ga<sub>2</sub>O<sub>3</sub>

$\beta$ -Ga<sub>2</sub>O<sub>3</sub> has a monoclinic structure, which contains two Ga and three O nonequivalent sites forming one tetrahedral and one octahedral structure around the Ga sites.<sup>[1,16]</sup> When deposited on *c*-plane sapphire,  $\beta$ -Ga<sub>2</sub>O<sub>3</sub> grows with the (−201) orientation.<sup>[17]</sup> The structure exhibits six in-plane rotational domains, rotated by 60° around the [−201] direction, caused by twofold symmetry in  $\beta$ -Ga<sub>2</sub>O<sub>3</sub> on top of the threefold symmetry substrate.<sup>[17–19]</sup> Current literature suggests that  $\beta$ -Ga<sub>2</sub>O<sub>3</sub> has a bandgap of around


L. T. Penman, Z. M. Johnston, P. R. Edwards, R. W. Martin, F. C. P. Massabuau  
Department of Physics  
SUPA, University of Strathclyde  
107 Rottenrow East, Glasgow G4 0NG, UK  
E-mail: lewis.penman@strath.ac.uk

Y. Oshima  
Research Center for Electronic and Optical Materials  
National Institute for Materials Science  
1-1 Namiki, Tsukuba 305-0044, Japan

C. McAleese  
Aixtron Ltd.  
Anderson Road, Swavesey, Cambridge CB24 4FQ, UK

P. Mazzolini, R. Fornari  
Department of Mathematical, Physical and Computer Sciences  
University of Parma  
Area delle Scienze 7/A, 43124 Parma, Italy

P. Mazzolini, M. Bosi, L. Seravalli, R. Fornari  
IMEM-CNR  
Area delle Scienze 37/A, 43124 Parma, Italy

 The ORCID identification number(s) for the author(s) of this article can be found under <https://doi.org/10.1002/pssb.202400615>.

© 2025 The Author(s). physica status solidi (b) basic solid state physics published by Wiley-VCH GmbH. This is an open access article under the terms of the Creative Commons Attribution License, which permits use, distribution and reproduction in any medium, provided the original work is properly cited.

DOI: 10.1002/pssb.202400615

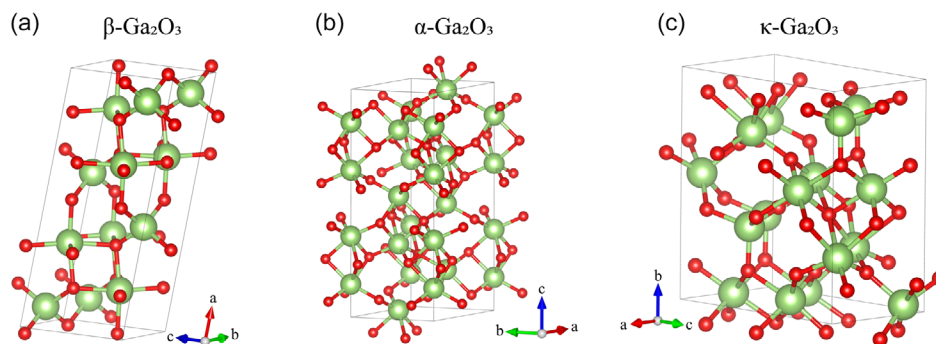


**Figure 1.** Unit cells of a)  $\beta$ -Ga<sub>2</sub>O<sub>3</sub>, b)  $\alpha$ -Ga<sub>2</sub>O<sub>3</sub>, and c)  $\kappa$ -Ga<sub>2</sub>O<sub>3</sub> represented using VESTA<sup>[13]</sup> with structural information taken from refs. [3,14,15].

4.8–5.0 eV<sup>[5,20–22]</sup> and a refractive index of 1.89.<sup>[23,24]</sup> Compared to the other polymorphs,  $\beta$ -Ga<sub>2</sub>O<sub>3</sub> currently possesses the most comprehensive literature on luminescence properties. The material exhibits broad luminescence over the UV and visible range, with components in the UV (3.2–3.6 eV),<sup>[25–27]</sup> blue (2.7–3.0 eV),<sup>[25,26,28–31]</sup> green (2.3–2.5 eV),<sup>[30]</sup> and red (1.7–1.9 eV) regions.<sup>[31–33]</sup> It is currently thought that the UV components result from the recombination of free electrons with self-trapped holes (STHs) located at O sites.<sup>[25,27,34]</sup> Luminescence in the blue region is generally attributed to shallow donor–acceptor pair (DAP) transitions with associated defects being Ga vacancies ( $V_{\text{Ga}}$ ), Ga–O divacancies ( $V_{\text{Ga}} + V_{\text{O}}$ ), or interstitial Ga ( $\text{Ga}_i$ ).<sup>[25,28,30]</sup> Deep DAP transitions are the currently accepted cause of green luminescence, where Ga and O vacancies ( $V_{\text{O}}$ ,  $V_{\text{Ga}}$ ) and interstitial O ( $\text{O}_i$ ) have all been proposed as the defects involved.<sup>[30]</sup> Lastly, red luminescence has been attributed to levels resulting from N, Fe, and Cr impurities.<sup>[31–33]</sup> Additionally, Onuma et al.<sup>[25]</sup> and Cho et al.<sup>[26]</sup> conducted temperature-dependent luminescence studies of undoped  $\beta$ -Ga<sub>2</sub>O<sub>3</sub> and found that the UV and blue emission peaks follow the conventional relation between emission and temperature first outlined by Varshni.<sup>[35]</sup> Also, Onuma et al. reported how the addition of dopants (Si, Mg) modify the luminescence of  $\beta$ -Ga<sub>2</sub>O<sub>3</sub> creating transitions that cause a visible reduction in overall luminescence as temperature decreases compared to undoped samples, as well as having an impact on crystal orientation.<sup>[25]</sup>

## 2.2. $\alpha$ -Ga<sub>2</sub>O<sub>3</sub>

$\alpha$ -Ga<sub>2</sub>O<sub>3</sub> is a metastable phase of Ga<sub>2</sub>O<sub>3</sub> which has gained interest for its wider bandgap and isomorphism with other sesquioxides.<sup>[36]</sup> It has a rhombohedral (corundum) structure containing one Ga and one O nonequivalent site creating a structure comprising of only octahedral sites.<sup>[1,14]</sup> When deposited on *c*-plane sapphire,  $\alpha$ -Ga<sub>2</sub>O<sub>3</sub> exhibits (0001) orientation.<sup>[35]</sup> This phase exhibits the widest bandgap among all polymorphs, around 5.1–5.6 eV,<sup>[5,21,22,38–40]</sup> and a refractive index of 1.74–1.95.<sup>[24,38,41]</sup> Compared with  $\beta$ -Ga<sub>2</sub>O<sub>3</sub>, less research effort has focused on  $\alpha$ -Ga<sub>2</sub>O<sub>3</sub>, but points for comparison do exist. Similar to  $\beta$ -Ga<sub>2</sub>O<sub>3</sub>,  $\alpha$ -Ga<sub>2</sub>O<sub>3</sub> features a broad luminescence spectrum covering a similar region, with peaks in the UV (3.2–3.8 eV),<sup>[26,42–46]</sup> blue (2.7–3.0 eV),<sup>[26,42–45,47]</sup> and green (2.5–2.6 eV) regions.<sup>[26,42]</sup> A higher energy UV emission at

3.8 eV has been assigned to DAP caused by H impurities combining with  $V_{\text{Ga}}$  to form hydrogenated gallium vacancies ( $V_{\text{Ga}}-n\text{H}$  where  $n$  is the number of H atoms occupying the  $V_{\text{Ga}}$ ).<sup>[42]</sup> The lower energy UV emission has been attributed to STH.<sup>[43,45,47,48]</sup> Shallow DAP transitions caused by  $V_{\text{Ga}}$  and  $V_{\text{Ga}} + V_{\text{O}}$  have been attributed to the blue luminescence.<sup>[42,48,49]</sup> There has been tentative assignment of green emission to deep DAP transitions from  $V_{\text{Ga}}$  and  $V_{\text{O}}$  centers.<sup>[42]</sup> However, throughout all the literature reviewed, it is very common to note that these assignments were drawn by analogy to  $\beta$ -Ga<sub>2</sub>O<sub>3</sub> luminescence, which could lead to misinterpretation. Literature reports varying degrees of temperature dependence of the luminescence spectrum. Cho et al. reported strong temperature dependence in the lower UV peak at 3.47 eV with a reduction in intensity by a factor of 10 in addition to a redshift of  $\approx 0.09$  eV.<sup>[26]</sup> Meanwhile, Moriya et al. reported a varying peak intensity with Sn dopant concentration, with higher concentrations causing an increase in blue emission of  $\approx 2.9$  eV and a reduction in UV emission  $\approx 3.6$  eV.<sup>[47]</sup> The UV peak exhibited a temperature dependence in the form of a reduction of intensity from 100 to 300 K of a factor of 3, while the blue peak seems to exhibit no change with temperature.<sup>[47]</sup> Nicol et al. reported that the 3.8 eV luminescence line became dominant at temperatures  $< 100$  K, while the other lines remained unchanged.<sup>[42]</sup> Janzen conducted a temperature and orientation-dependent study using *p*-polarized light from a dual monochromated Xe lamp source, on trigonal  $\alpha$ -Ga<sub>2</sub>O<sub>3</sub> deposited on *m*-plane sapphire.<sup>[43]</sup> Janzen identified two luminescence peaks, the higher energy 3.6 eV peak decreased in intensity as temperature increased. At 300 K, the peak was only 30% as intense compared to the peak at 5 K along the *a*-direction; additionally, it only became predominant at temperatures  $< 40$  K during excitation. When excited along the *c*-direction, the temperature dependence was more pronounced, with the UV peak disappearing entirely at temperatures  $> 100$  K. Furthermore, Janzen identified a blue peak at  $\approx 2.78$  eV, which showed an intensity increase from 5 to 100 K, followed by a decrease from 100 to 300 K. These properties were observed in both excitation orientations.<sup>[43]</sup>

## 2.3. $\kappa$ -Ga<sub>2</sub>O<sub>3</sub>

$\kappa$ -Ga<sub>2</sub>O<sub>3</sub> is also a metastable phase of Ga<sub>2</sub>O<sub>3</sub> which has gained interest for its spontaneous polarization, which may be exploited

for preparing heterostructures with a 2D electron gas at their interface.<sup>[6,7]</sup> It has an orthorhombic structure with four Ga and six O nonequivalent sites, the planes of O atoms have a purely hexagonal symmetry while the Ga planes in between are made of either only (two) Ga octahedral sites or Ga octahedral and Ga tetrahedral sites so that a 4H stacking forms along the (001) direction when deposited on *c*-sapphire.<sup>[2,3]</sup> To maintain the correct Ga:O stoichiometry of 2:3, one-third of the Ga sites are empty in both planes. The filled octahedra and tetrahedra sites are not randomly distributed in their planes but arranged in regular ribbons, which in the case of heteroepitaxy on *c*-plane sapphire leads to formation of 120° rotational domains separated by (110) twin planes, which ultimately give rise to a pseudo-hexagonal structure consisting of three separate crystal orientations.<sup>[2,3]</sup> Current literature suggests a bandgap of around 4.7–5.0 eV,<sup>[21,50–55]</sup> with refractive index of 1.96,<sup>[55]</sup> as estimated from ellipsometry measurements of orthorhombic  $\epsilon$ -Ga<sub>2</sub>O<sub>3</sub> epilayers. Like the other polymorphs,  $\kappa$ -Ga<sub>2</sub>O<sub>3</sub> exhibits a broad luminescence spectrum, exhibiting UV (3.1–3.5 eV),<sup>[43,56,57]</sup> blue (2.6–3.0 eV),<sup>[43,45,56–60]</sup> green (2.3–2.4 eV),<sup>[43,56,59]</sup> and red luminescence (1.6–1.8 eV).<sup>[60]</sup> STH have been assigned to be the cause of UV emission.<sup>[43,56]</sup> V<sub>Ga</sub> shallow DAP transitions and V<sub>O</sub> deep DAP transitions are presumed to be responsible for blue and green emission,<sup>[43,56–59]</sup> respectively, but work by Janzen indicates that STH can cause blue emission.<sup>[43]</sup> Montedoro et al. identified peaks at 2.4, 2.75, 3.0, and 3.15 eV, and found that the 3.0 and 3.15 eV peaks showed a steady decrease in intensity when temperature was increased, both approximately halving in intensity from 80 to 280 K.<sup>[56]</sup> The 2.75 eV peak sees a much stronger temperature dependence, with an intensity decrease over the same temperature range of a factor of 4. Finally, the 2.4 eV peak shows a slightly weaker temperature dependence, with intensity decreasing by a factor of 3 over the 80–280 K range. Janzen's investigation identified a polarization dependence for a single domain  $\kappa$ -Ga<sub>2</sub>O<sub>3</sub> deposited on an  $\epsilon$ -GaFeO<sub>3</sub> substrate,<sup>[61]</sup> using the same apparatus as in the  $\alpha$ -Ga<sub>2</sub>O<sub>3</sub> investigation. Excitation along the *a*-direction produced peaks at 2.41, 2.70, 2.99, and 3.16 eV. Peaks at 2.70 and 2.99 eV were emitted during excitation along the *b*-direction.<sup>[43]</sup> During excitation along the *a*-axis, the temperature dependence of intensity was comparable to Montedoro et al. with one notable exception: a sharp increase at 250 K followed by a sharp decrease at 300 K, combined with a redshift throughout. In contrast, the *b*-axis study showed minimal dependence, with a slight increase at 250 K, an abrupt redshift at 300 K, and an increase in intensity.<sup>[43]</sup>

### 3. Experimental Section

#### 3.1. Samples

Five unintentionally doped Ga<sub>2</sub>O<sub>3</sub> films were investigated in this study: one sample in the  $\beta$ -phase, two samples in the  $\alpha$ -phase, and two samples in the  $\kappa$ -phase. The sample names, phases, and key features are summarized in **Table 1**.

The  $\beta$ -phase sample ( $\beta$ ) was grown by metal-organic chemical vapor deposition (MOCVD) on single-side polished *c*-plane sapphire, in an Aixtron 3 × 2" closed coupled showerhead reactor utilizing trimethylgallium (TMG) and O<sub>2</sub> precursors and N<sub>2</sub> carrier gas. The growth process began with the deposition of a thin nucleation layer at 700 °C, followed by the formation of an  $\approx$ 750 nm thick Ga<sub>2</sub>O<sub>3</sub> layer at 1050 °C and constant pressure of 100 mbar. The distance between the showerhead and the substrate could be adjusted dynamically during growth to minimize the pre-reaction of precursors, here a constant 9 mm gap was maintained throughout the growth. The thickness of the sample was obtained by usage of a known growth rate.

The  $\alpha$ -phase samples ( $\alpha_1$  and  $\alpha_2$ ) were grown on single-side polished *c*-plane sapphire by halide vapor-phase epitaxy (HVPE) in a horizontal quartz reactor at 520 °C under atmospheric pressure. O<sub>2</sub> and GaCl were used as the precursors. The GaCl was synthesized by a chemical reaction of metal Ga and HCl gas upstream in the reactor at 570 °C with N<sub>2</sub> was used as the carrier gas.<sup>[37]</sup> The thicknesses of both  $\alpha$ -phase samples were estimated using a growth rate obtained by analyzing sample cross sections.

The  $\kappa$ -phase sample  $\kappa_1$  was grown by HVPE on single-side polished *c*-plane sapphire with a TiO<sub>2</sub> interlayer, at a temperature of 550 °C in the same HVPE reactor used for the growth of samples  $\alpha_1$  and  $\alpha_2$ .<sup>[50]</sup> Finally, sample  $\kappa_2$  was grown by MOCVD on single-side polished *c*-plane sapphire in a proprietary horizontal reactor, using TMG and ultrapure H<sub>2</sub>O, with He as carrier gas at a temperature of 650 °C and pressure of 100 mbar.<sup>[62]</sup> This sample features a notable thickness gradient across its surface, with estimated thickness of 1100 nm in the gas inlet side and 600 nm at the gas outlet side, spaced about 2 cm. The thickness of  $\kappa_1$  was obtained using the same method as the  $\alpha$ -phase samples, while the thickness of  $\kappa_2$  was obtained by optical reflectometry.

We noted that lattice strain could affect the optical properties,<sup>[63]</sup> but given that all our samples consisted of 100 s nm thick films grown by heteroepitaxy, it could be assumed that they were fully relaxed.

Samples  $\alpha_1$  and  $\kappa_2$  were used for the Swanepool methods due to their well discernable fringes in transmittance spectra, while

**Table 1.** Summary of the of the samples investigated here and comparison with literature.

Sample name	Phase	Growth method	Orientation	Thickness <i>d</i> [nm]		Bandgap <i>E<sub>g</sub></i> [eV]		Refractive Index [ <i>n</i> ]	
				Target	Measured	Literature	This work	Literature	This work
$\beta$	$\beta$	MOCVD	(−201)	750	755 (3)	4.8–5.0 <sup>[5,20–22]</sup>	4.99 (4)	1.89–1.91 <sup>[23,24,55]</sup>	1.89 (1)
$\alpha_1$	$\alpha$	HVPE	(0001)	350	352 (3)	5.1–5.6 <sup>[5,21,22,38–40]</sup>	5.32 (9)	1.74–1.95 <sup>[24,38,41]</sup>	2.00 (1)
$\alpha_2$				1500	–		–		–
$\kappa_1$	$\kappa$	HVPE	{001}	1200	–	4.7–5.0 <sup>[21,50–55]</sup>	–	1.96 <sup>[53]</sup>	–
$\kappa_2$		MOCVD		600–1100	743 (5)		4.87 (4)		1.85 (1)

$\alpha_2$  and  $\kappa_1$  were chosen for photoluminescence (PL) due to their higher luminescence. Sample  $\beta$  was suitable for both techniques.

### 3.2. Spectrophotometry

UV-vis spectrophotometry was conducted using a Shimadzu UV-2600 spectrophotometer with ISR-2600Plus integrating sphere attachment. The typical illuminated area in the system was  $\approx 2 \times 5$  mm, and a bespoke sample holder reducing the illuminated area to a circle with diameter of  $\approx 1.8$  mm was fabricated to analyze sample  $\kappa_2$  to avoid the thickness gradient affecting the transmittance. We estimated that the transmittance had an absolute 0.5% uncertainty, and the wavelength had a 0.3 nm absolute uncertainty. The transmittance was used to obtain the optical bandgap  $E_g$ , refractive index  $n$ , and thickness  $d$  of the films. The films, being hundreds of nanometers thick, exhibited fringes in the high transmittance region, which we analyzed using the Swanepoel method.<sup>[64]</sup> This approach utilized the maxima and minima of fringes to fit two lines creating an envelope with the upper line known as  $T_M$  and the lower as  $T_m$  to the transmittance spectra. The refractive index  $n$  was calculated as a function of  $T_M$ ,  $T_m$ , and the refractive index of the substrate. Then with  $n$  and  $\lambda$ , the sample thickness  $d$  could then be determined where  $n$  and  $\lambda$  were adjacent maxima or minima of the fringes; for an in-depth example of the Swanepoel method in practice, we directed the readers to the work of Sánchez-González et al.<sup>[65]</sup>

The Cauchy equation, Equation (1)<sup>[66]</sup>

$$n = A + \frac{B}{\lambda^2} \quad (1)$$

was used to express a fit of refractive index  $n$  against wavelength  $\lambda$  with  $A$  and  $B$  being constants. The optical bandgap was extracted from the linear interpolation of a  $\alpha^2$  versus  $h\nu$  plot, as is customary for direct bandgap semiconductors.<sup>[67]</sup> We noted that  $\text{Ga}_2\text{O}_3$  was not a direct bandgap semiconductor but its flat valence band allowed it to be treated as a direct bandgap for this purpose.<sup>[68]</sup> The absorption coefficient  $\alpha$  was obtained from the transmittance  $T$  only and thickness  $d$  of the film using Equation (2).

$$\alpha = \frac{1}{d} \times \ln\left(\frac{1}{T}\right) \quad (2)$$

### 3.3. PL

A custom-built PL setup employing a Photon Systems HeAg 224.8 nm pulsed laser at a frequency of 20 Hz with a 100  $\mu\text{s}$  pulse length was utilized for this experiment. The sample was mounted on a cold stage which incorporated a He-based closed loop cryostat covering a temperature range of 20–300 K. The emitted light from the sample was directed to an Oriel 1/8 m spectrograph with a 400 lines per mm ruled diffraction grating blazed at 325 nm, and a cooled Andor CCD camera. A 280 nm long-pass filter was used at the opening aperture of the spectrometer to filter out reflected laser light. The spectrum was corrected for system response using a DH3 CAL Ocean Optics radiometrically calibrated UV-vis-(NIR) near-infrared light source. The acquired spectra were decomposed into Gaussians using the FitYK software package.<sup>[69]</sup>

In both UV-vis and PL, samples were subjected to incident light and measured along the growth direction.

## 4. Results and Discussion

The results from the UV-vis spectrophotometry investigation of samples  $\alpha_1$ ,  $\beta$ , and  $\kappa_2$  are summarized in Table 1 and Figure 2. Fringes are clearly visible for all samples in the high transmittance region, i.e., for wavelengths greater than  $\approx 300$  nm, with the fringe spacing inversely related to the film thickness. The peak transmittance is lower than expected,<sup>[19,38,51]</sup> this is due to the usage of single-side polished substrates. As can be seen in Table 1, the film thickness values obtained from the Swanepoel analysis are in excellent agreement with the sample specifications. In the case of sample  $\kappa_2$ , which exhibits a thickness gradient, the extracted thickness fits within the range of

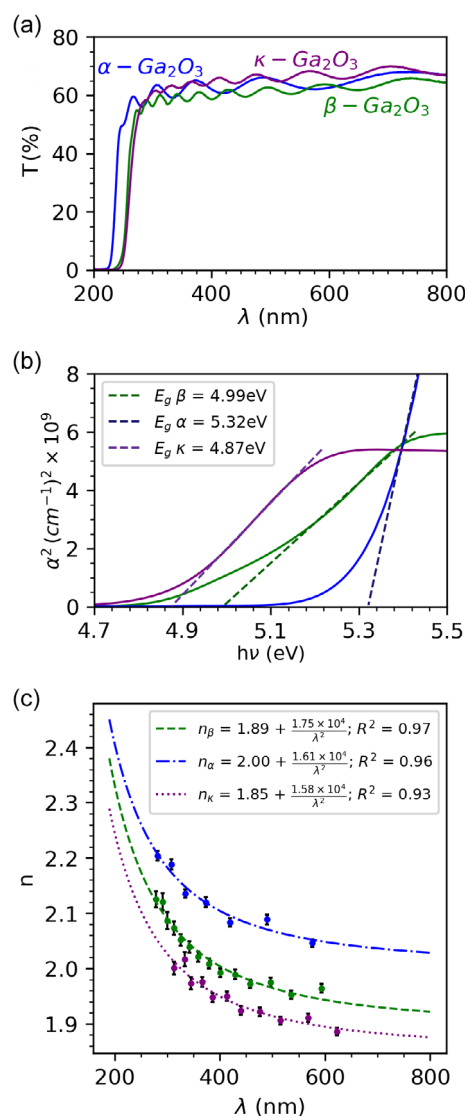


Figure 2. a) Transmittance plots, b)  $\alpha^2$  versus  $h\nu$  plot, and c) refractive index with Cauchy fit for the samples  $\beta$ ,  $\alpha_1$ , and  $\kappa_2$ .

expected thicknesses. These results demonstrate the strength of using transmittance methods for providing prompt feedback to growth.

Figure 2b shows the  $\alpha^2$  vs  $h\nu$  plots for each of the samples, allowing us to obtain the optical bandgap of each of the  $\text{Ga}_2\text{O}_3$  polymorphs; these values are summarized in Table 1. For  $\beta\text{-Ga}_2\text{O}_3$  with  $(-201)$  orientation, we obtain an  $E_g$  of  $4.99 \pm 0.04$  eV, which is in agreement with the literature.<sup>[5,20–22]</sup> Our data confirm that  $(0001)$  oriented  $\alpha\text{-Ga}_2\text{O}_3$  exhibits the widest bandgap among all three studied polymorphs,<sup>[5,21,22,38–40]</sup> with a value of  $5.32 \pm 0.09$  eV, which is in the upper region of reported values.<sup>[40]</sup> Finally, we obtain an  $E_g$  value of  $4.87 \pm 0.04$  eV for  $\{001\}$  oriented  $\kappa\text{-Ga}_2\text{O}_3$ , which is within the range of values reported in the literature.<sup>[21,50–55]</sup> With respect to the literature our data does agree that  $\alpha\text{-Ga}_2\text{O}_3$  possesses the largest  $E_g$  value, though we note that our study finds the  $E_g$  of  $\beta\text{-Ga}_2\text{O}_3$ , to be greater than  $\kappa\text{-Ga}_2\text{O}_3$  which is not always the case. The varying reports of  $E_g$  of the  $\beta$ - and  $\kappa$ -phase illustrate the anisotropy of the crystal properties, thus affecting how the  $E_g$  values exists with relation to each other.<sup>[5,20–22,43,50–55,63,70,71]</sup> Like the majority of papers that have been reviewed, we have used transmission measurements to obtain the bandgaps, although various analysis methods were employed within that body of studies, including  $\alpha^2$  versus  $h\nu$ ,  $(ah\nu)^2$  versus  $h\nu$ , or direct reading from transmittance. Meanwhile, Guemann et al. have estimated the  $E_g$  by observing the near-band-edge cathodoluminescence, and Segura et al. used both ellipsometry and absorption with a Elliott–Toyozawa model; both methods found agreement on the final result of 5.6 eV, the upper boundary of reported values.<sup>[5,40]</sup>

The Swanepoel method also allows the refractive index dispersion to be extracted for all three phases, as illustrated in Figure 2c. All the data points can be well fitted using the Cauchy equation. For  $\beta$ -phase, we obtain a refractive index of  $1.89 \pm 0.01$ , which is in excellent agreement with the findings of Rebien et al. and Zolnai et al. both using ellipsometry with photon energies ranging from 0.74 – 1.5 eV.<sup>[23,55]</sup> We observe a higher refractive index for  $\alpha\text{-Ga}_2\text{O}_3$  than  $\beta\text{-Ga}_2\text{O}_3$ , as predicted

theoretically by He et al.<sup>[24]</sup> The refractive index for  $\alpha\text{-Ga}_2\text{O}_3$  is  $2.00 \pm 0.01$ , close to the value from ellipsometry measurements which were taken over a range of 1.46–2.88 eV.<sup>[38]</sup> Finally, the refractive index of  $\kappa$ -phase is the lowest of all investigated phases, with a value of  $1.85 \pm 0.01$ . However, this deviates from the value of 1.96 obtained Zolnai et al.<sup>[55]</sup> with a 0.09 discrepancy at a comparable photon energy of 1.5 eV where  $n_{\kappa 2} \approx 1.87$ . While the close match of the other polymorphs with published reports gives confidence in our value, the discrepancy is notable. Perhaps this difference is due to the fact that we employ a different technique compared to Zolnai et al. who used ellipsometry, to obtain a dielectric value  $\epsilon$  which can be converted to a refractive index  $n$  using the relation  $\text{Re}(\epsilon) \approx n^2$ . Examining reports on dielectric values across polymorphs, these values are contradictory with reported refractive index results, in that they indicate the refractive index of  $\kappa\text{-Ga}_2\text{O}_3$  is lower than that of  $\beta\text{-Ga}_2\text{O}_3$ , which supports our findings with dielectric values of 9.85 for  $\kappa\text{-Ga}_2\text{O}_3$  and 10.2–12.4 for  $\beta\text{-Ga}_2\text{O}_3$ .<sup>[72,73]</sup>

The luminescence properties of samples  $\alpha_2$ ,  $\beta$ , and  $\kappa_1$  were then investigated by means of temperature-dependent PL over the 23–300 K range, as illustrated in Figure 3. Since we use above-bandgap excitation (224.8 nm, i.e., 5.5 eV) and the thickest samples (minimum thickness  $\approx 750$  nm), we can rule out any contribution from the substrate to the luminescence. To identify the contributions to the spectrum and enable comparison with the literature, the low-temperature spectrum of each polymorph was decomposed into several Gaussian lines—a common practice in existing literature<sup>[26,27,30,42,43,46,48,56,74]</sup>—and shown in the bottom plot of Figure 3. We have chosen to use four peaks to describe the fit which is consistent with literature.<sup>[30,48,56]</sup> Both  $\beta$ - and  $\kappa\text{-Ga}_2\text{O}_3$  exhibit peak shift, this has been highlighted with a black dot in Figure 3a,e.

For  $(-201)$ -oriented  $\beta\text{-Ga}_2\text{O}_3$ , in Figure 3a,b, we observe luminescence lines (at 23 K) centered at 2.5, 2.9, 3.3, and 3.6 eV—the increase of intensity below 2 eV comes from second order diffraction in the spectrometer. Based on the extensive literature on the luminescence of this polymorph, we attribute the peaks at 3.6 and 3.3 eV to STH.<sup>[27,70,75]</sup> The 2.9 and 2.5 eV peaks correspond

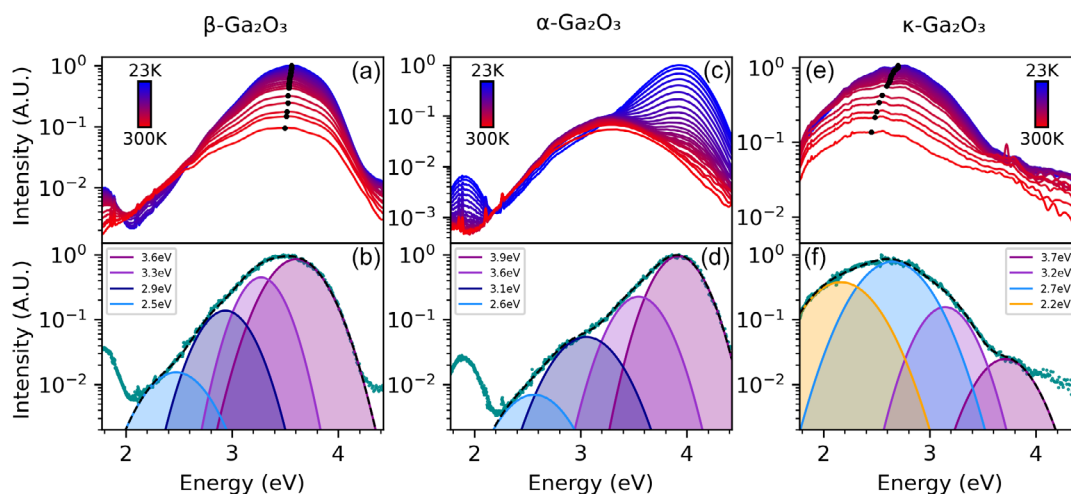


**Figure 3.** Temperature-dependent PL spectra of a)  $\beta\text{-Ga}_2\text{O}_3$  (sample  $\beta$ ), c)  $\alpha\text{-Ga}_2\text{O}_3$  (sample  $\alpha_2$ ), and e)  $\kappa\text{-Ga}_2\text{O}_3$  (sample  $\kappa_1$ ). Decompositions of the 23 K PL spectrum of b)  $\beta\text{-Ga}_2\text{O}_3$ , d)  $\alpha\text{-Ga}_2\text{O}_3$ , and f)  $\kappa\text{-Ga}_2\text{O}_3$ . For visibility, the peak position of each spectrum is marked with a black dot.

to DAP recombination between  $V_O$  acting as donors<sup>[29]</sup> and  $V_{Ga}$  or  $(V_{Ga} + V_O)$  as acceptors.<sup>[75]</sup> We observe a steady decrease in PL intensity by a factor of 10 as the temperature increase from 23 to 300 K. The PL spectrum intensity weakens with little change in the spectral shape as the temperature increases and exhibits a small peak redshift of  $\approx 0.12$  eV across the 23–300 K range.

In Figure 3c,d,  $\alpha$ -Ga<sub>2</sub>O<sub>3</sub> with (0001) orientation exhibits peaks (at 23 K) at 2.6, 3.1, 3.6, and 3.9 eV—the PL signal below 2 eV is an artefact coming from second-order diffraction in the spectrometer. We can see that as the temperature increases from 23 to 300 K, the 3.9 eV line intensity rapidly decreases by a factor of around 100 and the 3.6 eV line decreases by a factor of 10 while the other lines remain unchanged. This behavior is in strong contrast to what we observed for  $\beta$ -Ga<sub>2</sub>O<sub>3</sub>. Similar spectra and temperature dependence were observed by Nicol et al.<sup>[49]</sup> and Modak et al.<sup>[44]</sup> but they differ from observation from Janzen<sup>[43]</sup> where two distinct peaks can be observed in excitation along the *a*-direction and the maximum intensity being at a lower energy in excitation along the *c*-direction—we note however that Janzen was investigating the impact of polarization which could explain the discrepancies. The 3.9 eV peak is likely a DAP transition line involving H<sub>1</sub> as shallow donor and  $V_{Ga-nH}$  as acceptor, where H impurities are brought from the growth precursors.<sup>[42]</sup> The second UV peak at 3.6 eV is likely related to STH.<sup>[26,45]</sup> The peak at 3.1 eV could be assigned to shallow DAP transitions involving  $V_O$  donors and  $(V_{Ga} + V_O)$  acceptors and 2.6 eV to deep DAP transitions involving  $V_O$  donors and  $V_{Ga}$  or  $O_i$  acceptors. While these attributions are derived by analogy to the 2.9 and 2.5 eV lines of  $\beta$ -Ga<sub>2</sub>O<sub>3</sub>,<sup>[30,75]</sup> respectively, we note that Maruzane et al. conducted cathodoluminescence mapping of  $\alpha$ -Ga<sub>2</sub>O<sub>3</sub> which revealed that these luminescence lines increase in intensity in the vicinity of dislocations (as a result of point defect segregation), thus supporting a DAP transition interpretation.<sup>[46]</sup>

Finally, the luminescence of {001}-orientated  $\kappa$ -Ga<sub>2</sub>O<sub>3</sub> exhibits peaks at 2.2, 2.7, 3.2, and 3.7 eV (Figure 3e,f). We observe that, in comparison to  $\beta$ - and  $\alpha$ -Ga<sub>2</sub>O<sub>3</sub>, the lower energy components exhibit a greater contribution to the luminescence, as has been observed in the literature.<sup>[56,76]</sup> The PL spectrum of  $\kappa$ -Ga<sub>2</sub>O<sub>3</sub> gradually weakens with temperature, the 2.7 eV peak decreases intensity by a factor of 6 and both the 2.2 and 3.2 eV peaks only decrease intensity by a factor of 4 while the 3.7 eV peaks exhibit negligible change. There also appears to be a redshift of the spectrum of  $\approx 0.25$  eV as the temperature increases from 23 to 300 K, in agreement with literature.<sup>[43,53,55,76]</sup> The 3.7 eV peak can be tentatively attributed to H-related defects (e.g.,  $V_{Ga-nH}$  deep acceptors which facilitate recombination with electrons from either the conduction band or  $V_{O-H}$ , a hydrogenated oxygen vacancy) as shown by Mazzolini et al.<sup>[53]</sup> Since samples  $\alpha_2$  and  $\kappa_1$  were both grown by HVPE, i.e., employing HCl gas, it is perhaps not surprising if both samples exhibit a H-related luminescence line. The 3.2 eV peak has been ascribed to STH,<sup>[56]</sup> additionally the 2.7 eV peak agrees with that seen in literature caused by hydrogenated deep acceptors  $(V_{Ga-2H})$ .<sup>[53]</sup> In  $\kappa$ -Ga<sub>2</sub>O<sub>3</sub> studies both the 3.7 and 2.7 eV peaks have been assigned by analogy to  $\beta$ -Ga<sub>2</sub>O<sub>3</sub>, but this attribution has been backed up by theoretical calculations.<sup>[53]</sup> Finally, the 2.2 eV peak has not been reported in literature, but it has been observed in other polymorphs.<sup>[75]</sup>

## 5. Conclusion

The optical properties of  $\beta$ -,  $\alpha$ -, and  $\kappa$ -Ga<sub>2</sub>O<sub>3</sub> polymorphs have been investigated. A systematic approach allowed us to highlight phase-specific optical properties. Analysis of the transmittance spectra revealed refractive indices of  $1.89 \pm 0.01$  ( $\beta$ ),  $2.00 \pm 0.01$  ( $\alpha$ ), and  $1.85 \pm 0.01$  ( $\kappa$ ), and optical bandgaps of  $4.99 \pm 0.04$  eV ( $\beta$ ),  $5.32 \pm 0.09$  eV ( $\alpha$ ), and  $4.87 \pm 0.04$  eV ( $\kappa$ ). Temperature-dependent PL revealed that the emission spectrum of the polymorphs and their dependence with temperature differ significantly from each other with peaks at 2.5, 2.9, 3.3, and 3.6 eV ( $\beta$ -Ga<sub>2</sub>O<sub>3</sub>); 2.6, 3.1, 3.6, and 3.9 eV ( $\alpha$ -Ga<sub>2</sub>O<sub>3</sub>); and 2.2, 2.7, 3.2, and 3.7 eV ( $\kappa$ -Ga<sub>2</sub>O<sub>3</sub>). Our findings emphasize that deducing the optical properties of Ga<sub>2</sub>O<sub>3</sub> polymorphs by analogy to the well-documented  $\beta$ -Ga<sub>2</sub>O<sub>3</sub> could lead to misinterpretations such as an inaccurate defect characterization being made and then propagated in the literature and underline the necessity for detailed phase-specific investigations.

## Acknowledgements

The authors acknowledge support from the Engineering and Physical Sciences Research Council (grant nos. EP/W524670/1 and EP/V034995/1) and from the Rank Prize Undergrad Vacation scholarship. MB and RF acknowledge the financial support from PNRR-M4C2-11.1—Funded by the European Union-NextGenerationEU; Italian Ministry of University and Research Call for proposals n.104 of 02-02-2022-PRIN2022-ERC sector PE3 Project title: UV-C Sensors based on Gallium Oxide (USE GAO)-Project Code 2022A4AN2F-CUP CodeD53D23002180006 (grant decree no. 2022A4AN2F), dated 28/09/2023. The authors would also like to thank Indraneel Sanyal, Andrew Pakes, and Stuart Semple for their contributions to this work.

## Conflict of Interest

The authors declare no conflicts of interest.

## Data Availability Statement

The data that support the findings of this study are openly available from the University of Strathclyde KnowledgeBase at <https://doi.org/10.15129/61b028bc-643b-42ea-b55c-4f86b5ba56ca>.

## Keywords

gallium oxides, photoluminescences, polymorphs, semiconductors, transmittances, wide-bandgaps

Received: November 15, 2024

Revised: January 24, 2025

Published online:

- [1] S. J. Pearton, J. Yang, P. H. Cary IV, F. Ren, J. Kim, M. J. Tadjer, M. A. Mastro, *Appl. Phys. Rev.* **2018**, 5, 011301.
- [2] Y. Oshima, K. Kawara, T. Oshima, T. Shinohe, *Jpn. J. Appl. Phys.* **2020**, 59, 115501.
- [3] I. Cora, F. Mezzadri, F. Boschi, M. Bosi, M. Čaplovičová, G. Calestani, I. Dódony, B. Pécz, R. Fornari, *CrystEngComm* **2017**, 19, 1509.

- [4] M. Higashiwaki, *AAPPS Bull.* **2022**, *32*, 3.
- [5] F. Guemann, P. Nádaždy, K. Hušková, E. Dobročka, J. Priesol, F. Egyenes, A. Šatka, A. Rosová, M. Ťapajna, *Mater. Sci. Semicond. Process.* **2023**, *156*, 107289.
- [6] P. Ranga, S. B. Cho, R. Mishra, S. Krishnamoorthy, *Appl. Phys. Express* **2020**, *13*, 061009.
- [7] S. B. Cho, R. Mishra, *Appl. Phys. Lett.* **2018**, *112*, 162101.
- [8] E. Ahmadi, Y. Oshima, *J. Appl. Phys.* **2019**, *126*, 160901.
- [9] H. Y. Kang, M. J. Yeom, J. Y. Yang, Y. Choi, J. Lee, C. Park, G. Yoo, R. B. Kyu Chung, *Mater. Today Phys.* **2023**, *31*, 101002.
- [10] A. Barthel, J. Roberts, M. Napari, M. Frentrup, T. Huq, A. Kovács, R. Oliver, P. Chalker, T. Sajavaara, F. Massabuau, *Micromachines* **2020**, *11*, 1128.
- [11] X. Chen, F. Ren, S. Gu, J. Ye, *Photon. Res., PRJ* **2019**, *7*, 381.
- [12] J. Xu, W. Zheng, F. Huang, *J. Mater. Chem. C* **2019**, *7*, 8753.
- [13] K. Momma, F. Izumi, *J. Appl. Crystallogr.* **2011**, *44*, 1272.
- [14] M. Marezio, J. P. Remeika, *J. Chem. Phys.* **1967**, *46*, 1862.
- [15] S. Geller, *J. Chem. Phys.* **1960**, *33*, 676.
- [16] J. Åhman, G. Svensson, J. Albertsson, *Acta Crystallogr., Sect. C: Cryst. Struct. Commun.* **1996**, *52*, 1336.
- [17] S. Nakagomi, Y. Kokubun, *J. Cryst. Growth* **2012**, *349*, 12.
- [18] T. Oshima, T. Okuno, S. Fujita, *Jpn. J. Appl. Phys.* **2007**, *46*, 7217.
- [19] F. B. Zhang, K. Saito, T. Tanaka, M. Nishio, Q. X. Guo, *J. Cryst. Growth* **2014**, *387*, 96.
- [20] D. Thapa, J. Lapp, I. Lukman, L. Bergman, *AIP Adv.* **2021**, *11*, 125022.
- [21] V. D. Wheeler, N. Nepal, D. R. Boris, S. B. Qadri, L. O. Nyakiti, A. Lang, A. Koehler, G. Foster, S. G. Walton, *Chem. Mater.* **2020**, *32*, 1140.
- [22] H. Sun, K.-H. Li, C. G. T. Castanedo, S. Okur, G. S. Tompa, T. Salagaj, S. Lopatin, A. Genovese, X. Li, *Cryst. Growth Des.* **2018**, *18*, 2370.
- [23] M. Rebien, W. Henrion, M. Hong, J. P. Mannaerts, M. Fleischer, *Appl. Phys. Lett.* **2002**, *81*, 250.
- [24] H. He, R. Orlando, M. A. Blanco, R. Pandey, E. Amzallag, I. Baraille, M. Rérat, *Phys. Rev. B* **2006**, *74*, 195123.
- [25] T. Onuma, S. Fujioka, T. Yamaguchi, M. Higashiwaki, K. Sasaki, T. Masui, T. Honda, *Appl. Phys. Lett.* **2013**, *103*, 041910.
- [26] S. Cho, J. Lee, I.-Y. Park, S. Kim, *Mater. Lett.* **2002**, *57*, 1004.
- [27] M. Meißner, N. Bernhardt, F. Nippert, B. M. Janzen, Z. Galazka, M. R. Wagner, *Appl. Phys. Lett.* **2024**, *124*, 152102.
- [28] A. Lucheckko, V. Vasylytsiv, M. Kushlyk, D. Slobodzyan, M. Baláž, J. Cebulski, K. Szmuc, J. Szlezak, Y. Shpotyuk, *Appl. Nanosci.* **2023**, *13*, 5149.
- [29] L. Binet, D. Gourier, *J. Phys. Chem. Solids* **1998**, *59*, 1241.
- [30] Y. Nie, S. Jiao, S. Li, H. Lu, S. Liu, S. Yang, D. Wang, S. Gao, J. Wang, Y. Li, *J. Alloys Compd.* **2022**, *900*, 163431.
- [31] G. Naresh-Kumar, H. MacIntyre, S. Subashchandra, P. R. Edwards, R. W. Martin, K. Daivasigamani, K. Sasaki, A. Kuramata, *Phys. Status Solidi B* **2021**, *258*, 2000465.
- [32] T. Zhang, J. Lin, X. Zhang, Y. Huang, X. Xu, Y. Xue, J. Zou, C. Tang, *J. Lumin.* **2013**, *140*, 30.
- [33] E. Nogales, J. A. García, B. Méndez, J. Piqueras, *J. Appl. Phys.* **2007**, *101*, 033517.
- [34] Y. K. Frodason, K. M. Johansen, L. Vines, J. B. Varley, *J. Appl. Phys.* **2020**, *127*, 075701.
- [35] Y. P. Varshni, *Physica* **1967**, *34*, 149.
- [36] Y. Oshima, E. Ahmadi, *Appl. Phys. Lett.* **2022**, *121*, 260501.
- [37] Y. Oshima, K. Kawara, T. Oshima, M. Okigawa, T. Shinohe, *Semicond. Sci. Technol.* **2020**, *35*, 055022.
- [38] J. W. Roberts, P. R. Chalker, B. Ding, R. A. Oliver, J. T. Gibbon, L. A. H. Jones, V. R. Dhanak, L. J. Phillips, J. D. Major, F. C.-P. Massabuau, *J. Cryst. Growth* **2019**, *528*, 125254.
- [39] D. Shinohara, S. Fujita, *Jpn. J. Appl. Phys.* **2008**, *47*, 7311.
- [40] A. Segura, L. Artús, R. Cuscó, R. Goldhahn, M. Feneberg, *Phys. Rev. Mater.* **2017**, *1*, 024604.
- [41] *CRC Handbook of Chemistry and Physics* (Eds: R. Weast, M. Astle) 63rd ed., CRC Press, Boca Raton, FL **1982**.
- [42] D. Nicol, Y. Oshima, J. W. Roberts, L. Penman, D. Cameron, P. R. Chalker, R. W. Martin, F. C.-P. Massabuau, *Appl. Phys. Lett.* **2023**, *122*, 062102.
- [43] B. M. Janzen, *Vibrational and Optical Properties of Gallium Oxide Polymorphs*, Doctoral Thesis, Technische Universität Berlin **2024**.
- [44] S. Modak, J. S. Lundh, N. S. Al-Mamun, L. Chernyak, A. Haque, T. Q. Tu, A. Kuramata, M. J. Tadjer, S. J. Pearton, *J. Vac. Sci. Technol., A* **2022**, *40*, 062703.
- [45] S. Shapenkov, O. Vyvenko, E. Ubyivovk, O. Medvedev, G. Varygin, A. Chikiryaka, A. Pechnikov, M. Scheglov, S. Stepanov, V. Nikolaev, *Phys. Status Solidi A* **2020**, *217*, 1900892.
- [46] M. Maruzane, Y. Oshima, O. Makydonska, P. R. Edwards, R. W. Martin, F. C.-P. Massabuau, *J. Phys. D: Appl. Phys.* **2024**, *58*, 03LT02.
- [47] R. Moriya, J. Kikawa, S. Mouri, T. Shinohe, S. Xiao, H. Miyake, T. Araki, *Phys. Status Solidi B* **2022**, *259*, 2100598.
- [48] L. Ghadbeigi, J. Cooke, G. T. Dang, T. Kawaharamura, T. Yasuoka, R. Sun, P. Ranga, S. Krishnamoorthy, M. A. Scarpulla, B. Sensale-Rodriguez, *J. Electron. Mater.* **2021**, *50*, 2990.
- [49] D. Nicol, S. Reynolds, K. Barr, J. W. Roberts, J. J. Jarman, P. R. Chalker, F. C.-P. Massabuau, *Phys. Status Solidi B* **2024**, *261*, 2300470.
- [50] Y. Oshima, E. G. E. G. Villora, Y. Matsushita, S. Yamamoto, K. Shimamura, *J. Appl. Phys.* **2015**, *118*, 085301.
- [51] Z. Fei, Z. Chen, W. Chen, S. Chen, Z. Wu, X. Lu, G. Wang, J. Liang, Y. Pei, *J. Alloys Compd.* **2022**, *925*, 166632.
- [52] J. Lee, H. Kim, L. Gautam, M. Razeghi, *Crystals* **2021**, *11*, 446.
- [53] P. Mazzolini, J. B. Varley, A. Parisini, A. Sacchi, M. Pavesi, A. Bosio, M. Bosi, L. Seravalli, B. M. Janzen, M. N. Marggraf, N. Bernhardt, M. R. Wagner, A. Ardenghi, O. Bierwagen, A. Falkenstein, J. Kler, R. A. De Souza, M. Martin, F. Mezzadri, C. Borelli, R. Fornari, *Mater. Today Phys.* **2024**, *45*, 101463.
- [54] S. Seacat, J. L. Lyons, H. Peelaers, *Appl. Phys. Lett.* **2020**, *116*, 232102.
- [55] Z. Zolnai, P. Petrik, A. Németh, J. Volk, M. Bosi, L. Seravalli, R. Fornari, *Appl. Surf. Sci.* **2023**, *636*, 157869.
- [56] V. Montedoro, A. Torres, S. Dadgostar, J. Jimenez, M. Bosi, A. Parisini, R. Fornari, *Mater. Sci. Eng., B* **2021**, *264*, 114918.
- [57] A. Y. Polyakov, V. I. Nikolaev, A. I. Pechnikov, S. I. Stepanov, E. B. Yakimov, M. P. Scheglov, I. V. Shchemerov, A. A. Vasilev, A. A. Kochkova, A. V. Chernykh, A. V. Chikiryaka, S. J. Pearton, *APL Mater.* **2022**, *10*, 061102.
- [58] J. Lee, H. Kim, L. Gautam, K. He, X. Hu, V. P. Dravid, M. Razeghi, *Photonics* **2021**, *8*, 17.
- [59] M. Pavesi, F. Fabbri, F. Boschi, G. Piacentini, A. Baraldi, M. Bosi, E. Gombia, A. Parisini, R. Fornari, *Mater. Chem. Phys.* **2018**, *205*, 502.
- [60] V. I. Nikolaev, S. I. Stepanov, A. I. Pechnikov, S. V. Shapenkov, M. P. Scheglov, A. V. Chikiryaka, O. F. Vyvenko, *ECS J. Solid State Sci. Technol.* **2020**, *9*, 045014.
- [61] H. Nishinaka, O. Ueda, D. Tahara, Y. Ito, N. Ikenaga, N. Hasuie, M. Yoshimoto, *ACS Omega* **2020**, *5*, 29585.
- [62] M. Bosi, L. Seravalli, P. Mazzolini, F. Mezzadri, R. Fornari, *Cryst. Growth Des.* **2021**, *21*, 6393.
- [63] R. Zhang, M. Li, G. Wu, L. Li, Z. Zhang, K. Liang, W. Shen, *Results Phys.* **2023**, *52*, 106916.
- [64] R. Swanepoel, *J. Sci. Instrum.* **1983**, *16*, 1214.
- [65] J. Sánchez-González, A. Díaz-Parralero, A. L. Ortiz, F. Guiberteau, *Appl. Surf. Sci.* **2006**, *252*, 6013.

- [66] F. A. Jenkins, H. E. White, *Fundamentals of Optics*, 4th ed., McGraw-Hill Prims, New York, NY **2001**.
- [67] J. I. Pankove, *Optical Processes in Semiconductors*, Dover Publications Inc, New York, NY **1975**.
- [68] H. Peelaers, C. G. Van de Walle, *Appl. Phys. Lett.* **2017**, *111*, 182104.
- [69] M. Wojdyr, *J. Appl. Crystallogr.* **2010**, *43*, 1126.
- [70] T. Gake, Y. Kumagai, F. Oba, *Phys. Rev. Mater.* **2019**, *3*, 044603.
- [71] Y.-C. Ho, G. Ye, C. Nnokwe, V. Kuryatkov, J. Warzywoda, L. Grave de Peralta, R. He, A. Bernussi, *ACS Omega* **2024**, *9*, 27963.
- [72] U. U. Muazzam, P. S. Chavan, R. Muralidharan, S. Raghavan, D. N. Nath, *Semicond. Sci. Technol.* **2022**, *37*, 055011.
- [73] A. Fiedler, R. Schewski, Z. Galazka, K. Irmscher, *ECS J. Solid State Sci. Technol.* **2019**, *8*, Q3083.
- [74] K. Shimamura, E. G. E. G. Villora, T. Ujiie, K. Aoki, *Appl. Phys. Lett.* **2008**, *92*, 201914.
- [75] Q. D. Ho, T. Frauenheim, P. Deák, *Phys. Rev. B* **2018**, *97*, 115163.
- [76] T. Hidouri, A. Parisini, S. Dadgostar, J. Jimenez, R. Fornari, *J. Phys. D: Appl. Phys.* **2022**, *55*, 295103.